Available online at www.sciencedirect.com
ScienceDirect
Journal of Power Sources 177 (2008) 123–130
JOURNAL OF POWER SOURCES
www.elsevier.com/locate/jpowsour

A micro-solid oxide fuel cell system as battery replacement

Anja Bieberle-Hütter[a,*], Daniel Beckel[a], Anna Infortuna[a], Ulrich P. Muecke[a], Jennifer L.M. Rupp[a], Ludwig J. Gauckler[a], Samuel Rey-Mermet[b], Paul Muralt[b], Nicole R. Bieri[c], Nico Hotz[c], Michael J. Stutz[c], Dimos Poulikakos[c], Peter Heeb[d], Patrik Müller[d], André Bernard[d], Roman Gmür[e], Thomas Hocker[e]

[a] *Nonmetallic Inorganic Materials, ETH Zurich, Wolfgang-Pauli-Strasse 10, HCI G 539, CH–8093 Zurich, Switzerland*
[b] *Ceramics Laboratory, EPFL, MXD station 12, CH–1015 Lausanne, Switzerland*
[c] *Laboratory of Thermodynamics in Emerging Technologies, ETH Zurich, Sonneggstr. 3, CH–8092 Zurich, Switzerland*
[d] *Institute for Micro- and Nanotechnology, Interstaatliche Hochschule für Technik Buchs NTB, Werdenbergstr. 4, CH–9471 Buchs, Switzerland*
[e] *Center for Computational Physics, Züricher Hochschule Winterthur, Technikumstr. 9, CH–8401 Winterthur, Switzerland*

Received 17 June 2007; received in revised form 23 October 2007; accepted 27 October 2007
Available online 13 November 2007

Abstract

The concept and the design of a micro-solid oxide fuel cell system is described and discussed. The system in this study is called the ONEBAT system and consists of the fuel cell PEN (positive electrode – electrolyte – negative electrode) element, a gas processing unit, and a thermal system. PEN elements of free-standing multi-layer membranes are fabricated on Foturan® and on Si substrates using thin film deposition and microfabrication techniques. Open circuit voltages of up to 1.06 V and power of 150 mW cm^{-2} are achieved at 550 °C. The membranes are stable up to 600 °C. The gas processing unit allows butane conversion of 95% and hydrogen selectivity of 83% at 550 °C in the reformer and efficient after-burning of hydrogen, carbon monoxide, and lower hydrocarbons in the post-combustor. Thermal system simulations prove that a large thermal gradient of more than 500 °C between the hot module and its exterior are feasible. The correlation between electrical power output – system size and thermal conductivity – heat-transfer coefficient of the thermal insulation material are shown. The system design studies show that the single sub-systems can be integrated into a complete system and that the requirements for portable electronic devices can be achieved with a base unit of 2.5 W and a modular approach.

Keywords: Micro-solid oxide fuel cell; Thin film deposition; Microfabrication; Gas processing; Thermal system

1. Introduction

State-of-the-art solid oxide fuel cell (SOFC) systems are designed for stationary applications in high power range, i.e. several 100 kW to the MW region, such as systems from Siemens-Westinghouse and Rolls Royce, or for power outputs of 1–20 kW, such as the systems from HEXIS, Ceramic Fuel Cells Limited, Versa Power or Topsoe Fuel Cells. Due to the higher power density of SOFC systems compared to other fuel cell types, SOFC systems were recently also proposed for portable applications with power ranges of about 20–250 W, such as introduced by Adaptive Materials and Mesoscopic Devices. The technology for all these systems is based on thick film and bulk processing and the systems have an overall size between a shoe box and a small truck.

Driven by the high power densities of SOFC systems as well as progress in thin film technology and microfabrication, the idea of a so-called micro-SOFC (μ-SOFC) was very recently investigated [1–5]. A μ-SOFC is foreseen for lower power applications in the range of 1–20 W as battery replacement in small electronic devices, such as laptops, portable digital assistants, camcorders,

* Corresponding author. Tel.: +41 44 633 6826; fax: +41 44 632 1132.
E-mail addresses: anja.bieberle@mat.ethz.ch (A. Bieberle-Hütter), jennifer.rupp@mat.ethz.ch (J.L.M. Rupp), ludwig.gauckler@mat.ethz.ch (L.J. Gauckler), samuel.rey-mermet@epfl.ch (S. Rey-Mermet), paul.muralt@epfl.ch (P. Muralt), hotz@ltnt.iet.mavt.ethz.ch (N. Hotz), dimos.poulikakos@ltnt.iet.mavt.ethz.ch (D. Poulikakos), peter.heeb@ntb.ch (P. Heeb), andre.bernard@ntb.ch (A. Bernard), gmr@zhwin.ch (R. Gmür), thomas.hocker@zhwin.ch (T. Hocker).

0378-7753/$ – see front matter © 2007 Elsevier B.V. All rights reserved.
doi:10.1016/j.jpowsour.2007.10.092

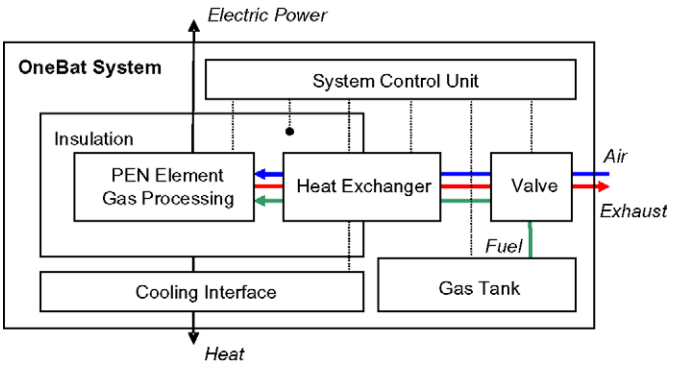

Fig. 1. The ONEBAT μ-SOFC system.

medical implements, industrial scanners, or battery chargers. Up to four times higher energy densities per volume and specific energy per weight are anticipated for these μ-SOFC systems compared to state-of-the-art rechargeable batteries such as Li-ion and Ni metal hydride batteries. The manufacture of these μ-SOFCs is based on thin film technology, microfabrication, and advanced packaging fulfilling complex thermal requirements [22,23,24]. So far, the development of such systems is in research status and to date the published data mainly relates to the first step of producing a micro fabricated fuel cell based on free-standing thin film SOFC membranes [3–5,25,26]. In this paper, for the first time a design for a μ-SOFC *system* consisting of a micro fabricated fuel cell, a gas processing unit and the thermal system is proposed. The different sub-systems are discussed in detail and a concept for the system integration is outlined.

2. The ONEBAT system

"ONEBAT" is the acronym for the μ-SOFC system described in this study. The system is designed with a base unit of 2.5 W electrical energy output and an overall volume smaller than 65 cm^3. The hot part of the system is at 350–550 °C while the exterior of the system remains at a safe handling temperature of below 35 °C. The system consists of a number of so-called PEN elements (positive electrode – electrolyte – negative electrode), i.e. the fuel cell stack, a gas processing unit composed of fuel reformer and exhaust gas post-combustor, a thermal system composed of a fuel and a air pre-heating unit, heat exchanger and insulation. Elements, such as gas tank, valve, and system control unit (SCU) are regarded as add-in products and are named external elements. Electrical peaks and start-up surge are managed by an electrical buffer, e.g. a super-capacitor. Fig. 1 shows a schematic illustration of the design of the ONEBAT system.

The system design foresees the PEN element to be packaged between two substrates, made from Si-single crystal or Foturan®. This sub-package is referred to as the unit-element (Fig. 2). The gas processing unit is subdivided into the gas preprocesser (reformer) and gas post-processor (post-combustor). A reformer and a post-combustor are placed before and after the unit-element, respectively, and are conceived as modular elements that can be repeated. The insulation encapsulates the micro-system. A micro heat exchanger exchanges the heat between the hot exhaust gas and the cold inflowing steam, such that the temperatures of the fluids at the inlet and outlet terminals are maintained as originally specified.

The modularity of the system enables adapting it to different power needs. One single modular element is sized for 2.5 W. By simply repeating these elements, it is possible to address higher power needs for more demanding portable application. The integration of the above mentioned components as well as the micro-system fabrication make use of various well-established processes in micro-technology, such as thin film deposition, photolithography, and wafer bonding.

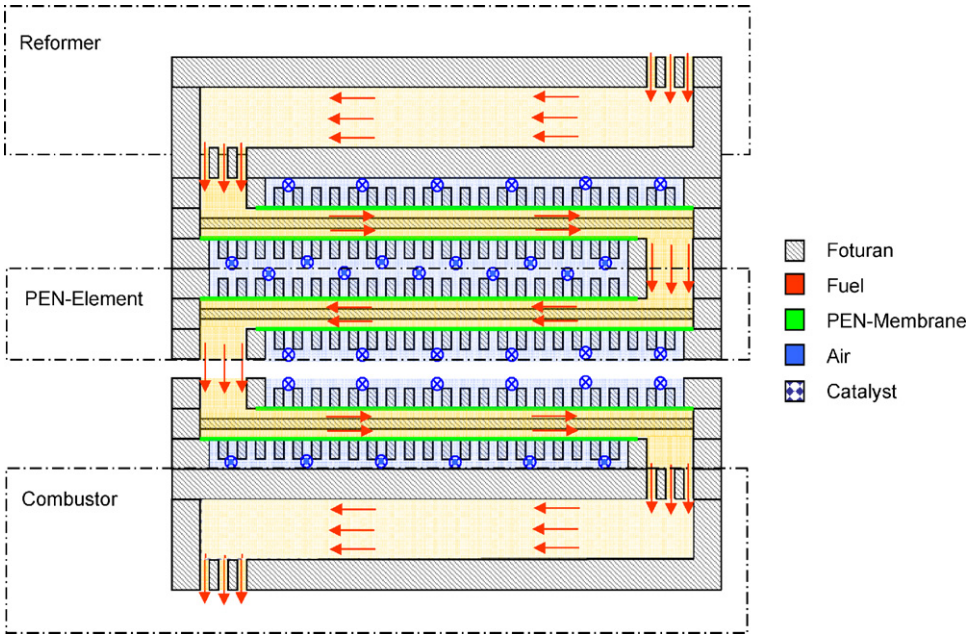

Fig. 2. A unit-element of the ONEBAT system.

3. The PEN element (positive electrode – electrolyte – negative electrode)

The heart of the ONEBAT system, i.e. the PEN, was fabricated on two different substrate materials: Foturan® and Silicon (Si). Foturan® is a special material that can be directly micro patterned, while Si is the usual material for micro processing of semiconductors and power switches. Both materials have been adopted in the study in order to check their feasibility for μ-SOFC application.

3.1. Experimental

3.1.1. Foturan® based cell

Foturan® is a photostructurable glass-ceramic that can be micro patterned by hydrofluoric acid (HF) etching [6]. Double-side polished wafers (Foturan®, Mikroglas, Mainz, Germany) with 100 mm diameter and 300 μm thickness were used as substrates.

To build up the fuel cell on the wafer, 100 nm thick chromium (Cr)/platinum (Pt) contact pads are radio frequency (RF) sputtered on the substrate surface. The areas where the membranes shall be released are UV-irradiated. Afterwards, the wafer is cut into chips of 24 mm × 24 mm containing anode contacts for three cells each. The platinum anode with a thickness of ∼50 nm is sputtered. The electrolyte consisting of 8 mol% yttria-stabilized zirconia (YSZ) of a thickness of ∼550 nm is prepared by pulsed laser deposition (PLD) and the cathode is prepared using spray pyrolysis ($La_{0.6}Sr_{0.4}Co_{0.2}Fe_{0.8}O_3$ with a thickness of ∼200 nm [7,8]. After thin film deposition, the chips are annealed at 600 °C in order to crystallize the thin films and the UV-exposed areas of the substrate. While the thin films are protected with a polymer coating, the crystalline areas of the chips are back etched with 10% HF in order to release the membranes. Finally, the cells are electrically contacted using Pt wires, Pt paste, and ceramic glue. The chips are integrated in a test rig for electrical measurement. For testing the cells, the gas at the cathode was air and the anode gas used was a hydrogen nitrogen mixture (H_2:N_2 = 1:4) humidified with a water bubbler. The voltage–current (*U–I*) characteristics of the cells were measured with a potentiostat (IM6, Zahner, Kronach, DE). The exact cell area was determined after testing by breaking the cells and analysing them by SEM. More details of each process step are given in [9–11].

3.1.2. Silicon-based cell

The Si-based cells also consist of free-standing membranes of similar materials as described for the Foturan® based cell. However, the cells are fabricated with a supporting grid to reinforce the free-standing membrane. A similar design concept as proposed in [12] was adopted. The metal grid allows for increasing the buckling limit in a single compartment of the mesh. The supporting grid is made of electrochemically deposited nickel, and has the advantage of serving at the same time as current collector on the anode side. All thin films used in the Si-based cells are deposited by reactive magnetron sputtering. Details on the design and the processing of the Si-based cells are described in [13].

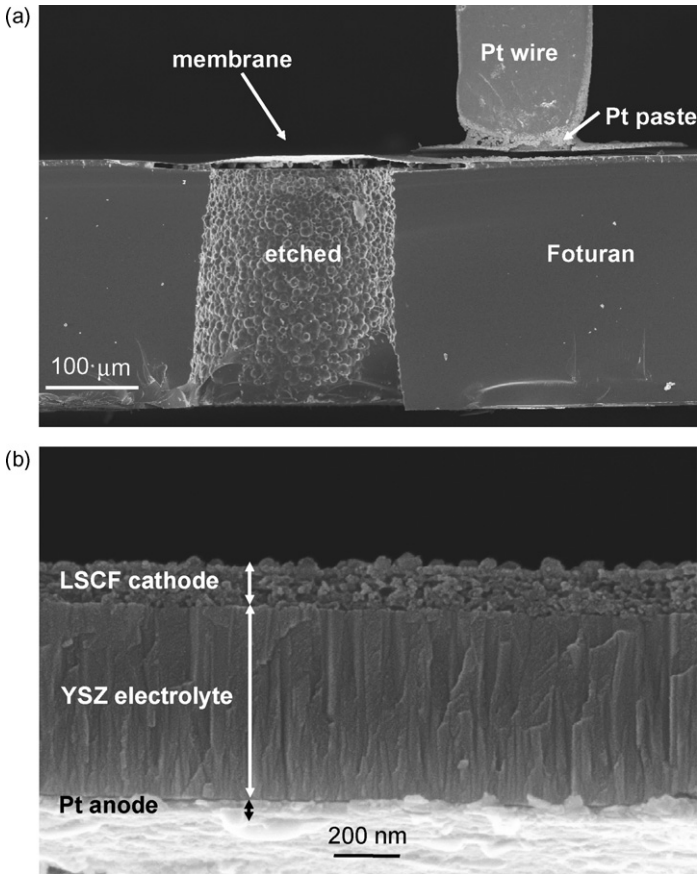

Fig. 3. (a) SEM cross-section view of a μ-SOFC on a Foturan® substrate. The cathode current collector (Pt wire and Pt paste) detached during breaking of the cell for SEM analysis. Some under-etching was observed below the membrane for this cell; (b) blow-up view of the membrane.

3.2. Results

3.2.1. Foturan® based cell

A cross-section SEM image of a free-standing Pt (sputtered)/YSZ (PLD)/LSCF (spray pyrolysis) cell on a Foturan® substrate is shown in Fig. 3. Fig. 3a shows the entire cross-section including contacts. Some under-etching of the membrane can be detected for this cell. Please note that the performance data is always based on the real cell area that is determined by SEM. The Pt contact in Fig. 3a is detached during the breaking of the cell for SEM analysis. Fig. 3b shows a blow-up of the membrane. The Pt anode and the LSCF cathode are forming nanoporous electrodes that adhere well to the electrolyte. The YSZ electrolyte is columnar with elongated grains perpendicular to the substrate surface.

U–I curves of the cell were recorded between 550 and 400 °C. The open circuit voltages (OCV) of cell 1 with a single PLD YSZ electrolyte were between 590 and 730 mV and power densities of 1.9, 15 and 39 mW cm^{-2} were measured at 400, 500 and 550 °C, respectively (Fig. 4). In cell 2, a second YSZ electrolyte

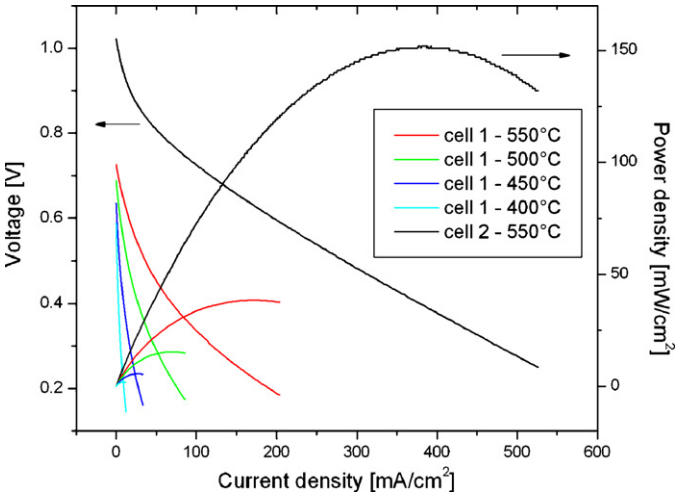

Fig. 4. *U–I* and performance curves of Foturan® based cells: cell 1: sputtered Pt anode (35–50 nm)/YSZ PLD electrolyte (550 nm)/LSCF spray pyrolysis cathode (200 nm); cell 2: sputtered Pt anode (35–50 nm)/YSZ PLD electrolyte (550 nm)/YSZ spray pyrolysis electrolyte (200 nm)/Pt paste cathode (10–20 μm).

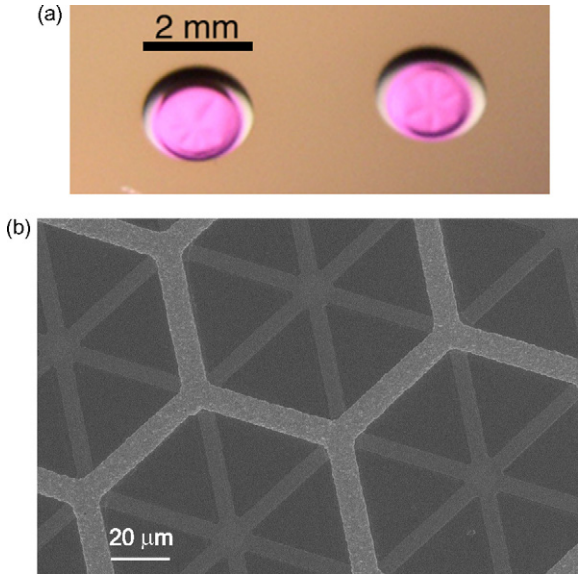

Fig. 6. (a) Light microscope image of a free-standing 2 mm wide CGO membrane; (b) SEM image of a Ni-grid grown on CGO layer, being part of a 5 mm wide membrane structure. Both images stem from silicon-based cells.

film prepared by spray pyrolysis was added. This layer improves the gas tightness of the electrolyte and OCV up to 1.06 V with a power density of 150 mW cm^{-2} was be obtained at 550 °C [10]. The fuel cell membranes with diameters up to 200 μm are stable up to 600 °C.

Impedance spectroscopy studies of the cells and of the single layers show that the contribution of the electrolyte resistance to the total cell resistance is negligible compared to the electrodes that are limiting the cell performance (Fig. 5). In particular the cathode limits the overall performance of the cells. The introduction of nanoporous LSCF with an average grain size around 20 nm as cathode material was an important step towards using high performance ceramic electrode materials and replacing expensive precious metal catalysts in μ-SOFC.

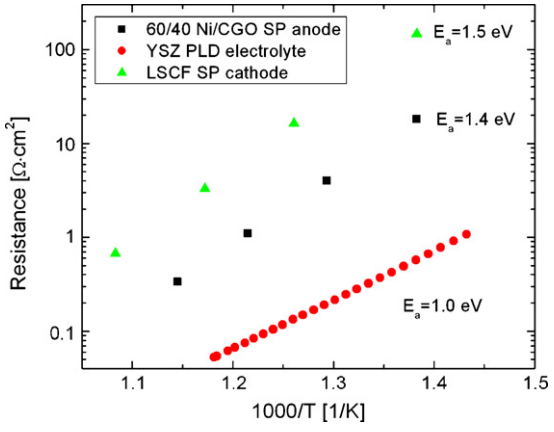

Fig. 5. Measured polarization resistances of anode and cathode as well as area specific resistance of electrolyte as a function of the temperature. While the resistances of the electrodes were determined by electrochemical impedance spectroscopy, the resistances of the electrolyte were calculated from 4-point conductivity measurement.

3.2.2. *Silicon-based cell*

The mechanical stability of free-standing cerium gadolinium oxide (CGO) membranes on Si substrates was investigated. Membranes of 2 mm diameter and a thickness of 200 nm were obtained (Fig. 6a). The membranes are crack-free up to 350 °C. With a nickel grid support structure having 90 μm spaces, line widths of 10 μm and a height of 5 μm (Fig. 6b), the mechanical stability is considerably increased and the reinforced membranes are mechanically stable up to 600 °C.

Several types of PEN devices were electrically tested in H_2/Ar gas mixtures on the anode side and air on the cathode side. PEN devices with a thickness of 1 μm consisting of single layer CGO electrolyte resulted in no OCV. With a second PEN including an additional 1 μm thick YSZ film on the anode side of the electrolyte, an OCV of 200 mV was obtained at 400 °C with a flow rate of H_2:Ar = 1:4.

4. The gas processing unit

4.1. *Experimental*

The gas processing unit consists of a butane-to-syngas processor and a post-combustor for fuel which did not react during the process. For the syngas catalyst production, ceria/zirconia nanoparticles (<10 nm) ($Ce_{0.5}Zr_{0.5}O_2$) with optional rhodium (Rh) doping are prepared in a one-step process by flame spray synthesis [14,15]. A homogenous mixture of 7.5 mg of such Rh/$Ce_{0.5}Zr_{0.5}O_2$ nanoparticles (0–2.0 wt% Rh) and 22.5 mg silica (SiO_2) sand (average diameter: 0.2 mm) formed a packed bed reactor. These porous packed beds were fixed in an Inconel tube between ceramic fiber plugs consisting of SiO_2. Butane from a liquid tank at 2.5 bar was mixed with compressed synthetic air and fed slightly above ambient pressure into the packed bed reactor heated by a tube furnace. The gas composition was analyzed

by a gas chromatograph (6890 GC, Agilent) coupled with a mass spectrometer (5975 MS, Agilent), using a HP-MOLSIV Agilent and a HP-PlotQ column (Agilent), respectively, as shown in [16].

For the post-combustor, $Ce_{0.5}Zr_{0.5}O_2$ nanoparticles with platinum doping are produced and tested in a similar way to that of $Rh/Ce_{0.5}Zr_{0.5}O_2$ nanoparticles.

4.2. Results

The capability of flame-made $Rh/Ce_{0.5}Zr_{0.5}O_2$ nanoparticles catalyzing the production of H_2- and CO-rich syngas from butane was investigated for different Rh loadings (0–2.0 wt% Rh) for a temperature range from 225 to 750 °C, using operational conditions that have been deduced from numerical simulations of methane processing [17–19]. Our results show that $Rh/Ce_{0.5}Zr_{0.5}O_2$ nanoparticles offer a very promising material for butane-to-syngas conversion with complete butane conversion (Fig. 7a) and a hydrogen selectivity of 85% (Fig. 7b) for the highest catalyst loading of 2.0 wt% Rh at the highest temperatures (600–750 °C). Even at lower temperatures, the catalytic performance of the $Rh/Ce_{0.5}Zr_{0.5}O_2$ nanoparticles was satisfactory for an application in a μ-SOFC system with butane conversion amounting to 95% and hydrogen selectivity to 83% at 550 °C (Fig. 7). By adjusting the operational parameters, such as fuel-to-air ratio, further improvement of the syngas production was possible, leading to butane conversion significantly higher than 90%, hydrogen selectivity above 85%, and carbon monoxide selectivity above 70% at 550 °C.

The flame-synthesized $Pt/Ce_{0.5}Zr_{0.5}O_2$ nanoparticles showed a very high conversion of hydrogen, carbon monoxide, and lower hydrocarbons at temperatures as low as 550 °C. Therefore, the feasibility of $Pt/Ce_{0.5}Zr_{0.5}O_2$ nanoparticles used in a packed bed reactor as a catalyst for post-combustion of the SOFC exhaust is feasible.

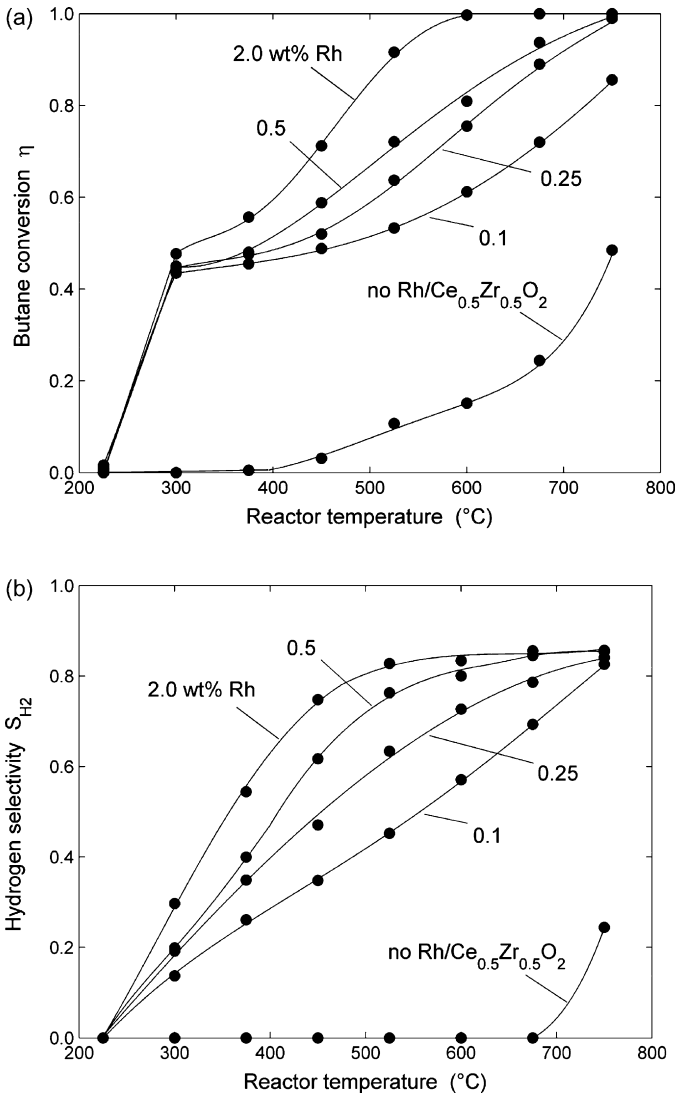

Fig. 7. The influence of Rh loading on $Ce_{0.5}Zr_{0.5}O_2$ on butane conversion η (ratio between converted butane and inlet butane) (a) and hydrogen selectivity S_{H_2} (produced hydrogen divided by the sum of produced hydrogen and water) (b) for an inlet C/O ratio $\phi = 0.8$. The solid lines through the data points are fitting data.

5. The thermal system

5.1. Model

By the use of thermal-flow finite element (FE) simulations, new concepts for the thermal management of a μ-SOFC system have been investigated. Due to the large surface-to-volume ratio, the high temperatures at which a SOFC operates are more difficult to control in micro-systems than in conventional ones. The large temperature gradient in the system from 350 to 550 °C internally to 35 °C externally requires excellent stack insulation as well as an efficient heat exchange between the exhaust gases and the inflowing anode and cathode gases. In addition, such large temperature drops per unit length induce large thermal stresses in different systems components. This might induce cracks and subsequently lead to leakage problems, both, within the stack and through its thermal insulation.

As shown in Fig. 8a, the 3D thermal-flow model of the ONEBAT system consists of the SOFC stack, the heat exchanger and different static insulation components. The model has been implemented into our in-house multi-physics FE-code "Seses" [27]. Within the flow domains, the Navier-Stokes equations for ideal gas flow are solved simultaneously with the energy-balance. The latter accounts for convective, conductive and radiative energy transportation, as well as for heat sinks and sources. Heat sinks and sources originate from several endothermic and exothermic (electro-) chemical reactions that take place on the cells, within the fuel reformer and within the post-combustion unit. The total amount of heat released, Q_{prod}, is given by the difference between the "chemical input", P_{chem}, based on the total oxidation of the fuel gas and the electrical power output, P_{el}, i.e. $Q_{prod} = P_{chem} - P_{el}$. For the static insulation parts, the heat conduction equation is resolved. As boundary condition at the surface of the housing, the convective heat flux, $j_{th} = \alpha(T - T_{amb})$, has been chosen, where T_{amb} is the ambient temperature and α is an adjustable heat-transfer coefficient. Depending on whether or not thermal radiation is

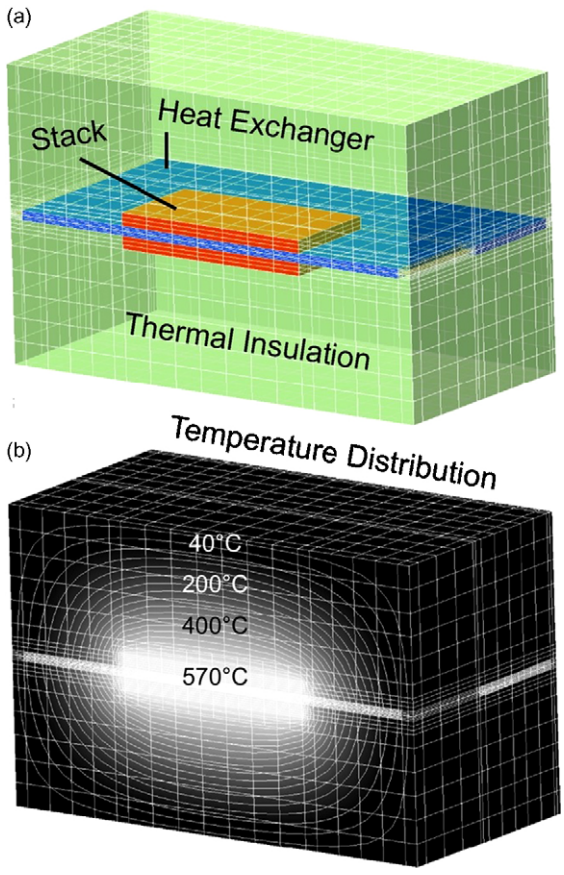

Fig. 8. Simulation of thermal system: (a) geometry of a 3D thermal-flow FE-model including stack, heat exchanger and static insulation components; (b) calculated temperature distribution under stationary operation conditions for an electrical power output of $P_{el} = 2.5\,W$ and a system size of $33\,mm \times 55\,mm \times 55\,mm$.

accounted for, a single simulation run takes from a few minutes up to about an hour.

5.2. Results

Fig. 8b shows a typical temperature distribution at steady-state conditions. White areas indicate the highest temperatures reached, whereas those in black show the lowest temperatures. When thermally well conducting stack components are used, the stack operates at a fairly homogeneously distributed temperature. However, the temperature rapidly drops towards the exterior. Note that the highest heat fluxes occur across the separating plates of the heat exchanger.

The required thermal conductivity, κ, of the static insulation is shown in Fig. 9, for different power outputs and boundary conditions. Calculations were made under the assumption that the electrical efficiency is relatively low, i.e. between 20% and 25%. At this limit, the system volume, V_{sys}, is controlled by the heat flux, I_{cond}, that needs to be dissipated to the exteriors. V_{sys} can be evaluated by assuming that I_{cond} follows Newton's cooling law, i.e. $I_{cond} = A_{sys}\ \alpha\ (T_{hou} - T_{amb})$. In this formular, A_{sys} is the surface area of the housing, α is the heat-transfer coefficient between housing and exteriors, T_{hou} and T_{amb} are

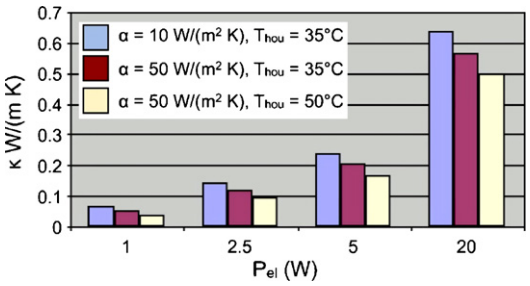

Fig. 9. Required thermal conductivities for the static insulation to achieve a stack temperature of 550 °C. The results were obtained for electrical power outputs P_{el} between 1 and 20 W, housing temperatures T_{hou} of 35 and 50 °C, and heat-transfer coefficients α (between the system and its surroundings) of 10 and 50 $W\,m^{-2}\,K^{-1}$.

the housing and ambient temperatures, respectively. To proceed further, T_{hou} is set to the maximum allowed housing temperature, I_{cond} is calculated from the global system energy-balance, and α is determined from how the ONEBAT system is connected with its surroundings. Newton's cooling law can then be solved for A_{sys} and from this result, the system volume V_{sys} can be found. The smaller V_{sys}, the smaller the thermal conductivity of the static insulation required to maintain a stack temperature of 550 °C. The results in Fig. 9 show the following trends: The smaller the electrical power output P_{el}, the larger the surface-to-volume ratio of the system and, hence, the smaller is the required κ-value of the static insulation. On the other hand, the smaller the heat-transfer coefficient α that is chosen, a larger system volume is required to dissipate the heat, hence, the higher allowable κ-value. Finally, it was found that the lower the allowable external housing temperature that is chosen, a much larger system size is required to dissipate the heat, with a consequentual allowable κ-value.

From these result it follows that for systems with smaller electrical power outputs, it is more difficult to find an insulation material with a low enough thermal conductivity. It can also be concluded from Fig. 9 that systems with low heat transfer to the surroundings due to a high electrical efficiency and low values of T_{hou} or low α, will lead to larger system volumes which are less demanding with respect to the heat-flow resistance of the static insulation.

6. Discussion

6.1. Foturan® versus silicon-based cells

The PEN element was fabricated on two different substrates, namely: Foturan® and Silicon. Both materials have distinct advantages and disadvantages.

Standard micro devices in MEMS technology are based on silicon as structural support. Deep silicon etching techniques, as needed for membrane fabrication, are well developed and can be applied quickly. Silicon is thermally very stable in the required temperature range; however, it is a brittle material and it is always covered with an oxide layer. One drawback could be its rather large thermal expansion coefficient difference to the ceramics of

the fuel cell's membranes of about 7 ppm K^{-1}, thus leading to thermal stresses in the range of 300–400 MPa in the ceramic film with a stiffness of around 100 GPa. It was found in this study that the mechanical stability of membranes can be increased by introducing a metal support grid and crack-free membranes with diameters of several millimeters were produced, which were larger than those of earlier results of 5 μm diameter membranes [20].

The Foturan® based cells have the advantage that the thermal expansion coefficient of the substrate is very close to that of the ceramic thin film materials and, hence, thermal expansion mismatch is not a major concern. Foturan® is a photostructurable glass-ceramic and can therefore be directly microstructured by wet etching using HF. The HF etching might, however, be a problem since it can easily attack the grain boundaries of the thin films. Thin film adhesion on Foturan® is excellent and due to its insulating behavior no electrically insulating layers such as silicon oxide or silicon nirtide are required. However, the maximum operating temperature of Foturan® is limited to 600 °C in the amorphous state and to 800 °C in the fully crystalline state due to softening. As the membrane materials of the PEN have to be annealed at about 600 °C and as this temperature is above the T_G of the glass-ceramic ($T_g \cong 460$ °C), stresses due to the membranes on the Foturan® might lead to warpage of the wafers. As crystallization of Foturan® also occurs above T_G, shrinkage of about 0.3% during crystallization is observed. Consequently, substrates become buckled after annealing; however, this is not a problem for μ-SOFC application.

In this study, it could be shown that with both substrates mechanically stable μ-SOFC PENs could be fabricated. These components were stable in the desired temperature range up to 600 °C. The stability of free-standing membranes was improved in case of the Si-based cells by using a metal support grid. The metal grid can also be integrated into a Foturan® based cell, if large membranes are considered.

The fuel cell performance was tested for both designs. It was found that Foturan® based cells performed better than Si-based cells. The reason was, however, not the substrate material, but the electrolyte and electrode materials, as well as thin film fabrication processes. In order to obtain high cell voltages, dense and pinhole free electrolyte films are required. This is very difficult to achieve with a single layer electrolyte and, in particular, with a vacuum deposition method which usually results in columnar grains in these thin films and, hence, gas diffusion through pinholes is highly feasible. Since the Si cells are all based on vacuum deposited thin films and sometimes are based on single electrolyte layers, the OCV was inferior compared to the Foturan® cells with multi-layer and partly sprayed thin films without columnar microstructure [21]. The double layer electrolyte cell with a PLD and a sprayed electrolyte thin film, as described in Section 3.2, yielded in the highest OCV of 1.06 V and a power output of 150 mW cm^{-2}.

It follows that both designs have distinct advantages and disadvantages. With both substrate materials free-standing membranes and well performing fuel cells can be fabricated. Differences in the performance of the fuel cells are not attributed to the substrate material. Hence, both designs are in principle feasible and processing reasons will be decisive in their choice.

6.2. The ONEBAT system

The results on the single sub-systems of the ONEBAT μ-SOFC system, i.e. the PEN, the gas processing unit, and the thermal system, were shown in the previous chapters. It was found that each single sub-system can be fabricated and works satisfactory. PEN elements of free-standing membranes of suitable size for μ-SOFC application were fabricated and are able to achieve performances to operate portable electronic devices when stacked. The gas processing unit is able to process the fuel gas to hydrogen that can directly fuel the SOFC at temperatures below 550 °C. Hydrogen and carbon monoxide in the exhaust gas of the SOFC can be converted to water and carbon dioxide by the post-combustor. The large temperature profile of more than 500 °C from the hot fuel cell to ambient surrounding can be managed according to simulations and thermal insulation experiments. The system design study showed that it is possible to integrate the different sub-systems into one complete system that is then fabricated by usual microfabrication techniques. A major concern for the system design is the manufacturing costs. Cost reductions can be achieved by using less layers for one repeat element and by fewer repeat elements in the system. This requires high current density of each element.

7. Summary and outlook

We have shown that a μ-SOFC system, such as the ONEBAT system, is technically feasible. Main results in the different subsystems, namely the PEN element, the gas processing unit, the thermal system, as well as the system design study proved that a μ-SOFC system is an attractive alternative to Li-ion batteries. In particular, it was shown that free-standing, multi-layer thin films of SOFC materials can be processed by thin film deposition and microfabrication. Free-standing ceramic membranes were reinforced by nickel grid structure to reach diameters of up to 5 mm. An open circuit voltage of 1.06 mV and a maximum power output of 150 mW cm^{-2} at 550 °C were obtained for single PEN elements. Lower operating temperatures and higher power output seem feasible by improving the electrolytes and specifically the catalytic activity of the cathodes. Taking the actual design parameters of our system we can anticipate a volume of 65 cm^3 for a 2.5 W system to be feasible when doubling the actual power density of the single membranes. High butane conversion in excess of 90% and hydrogen selectivity higher than 85% were demonstrated in a micro reformer at temperatures of 550 °C. Simulations and measurements of the thermal system confirmed that the targeted temperature profile of about 500 °C from internal to external temperatures is possible for such a small system. Design studies for integrating the different sub-systems into one complete system proved that a μ-SOFC system can be produced using conventional power electronic packaging technology. A demonstrable unit will be fabricated as next step.

Acknowledgements

This study was financially supported financially by the below-listed Swiss institutions:

- Comission for Technology and Innovation (CTI);
- Center of Competence Energy and Mobility (CCEM);
- Bundesamt für Energie (BfE);
- Swiss Electric Research (SER).

References

[1] D. Nikbin, Fuel Cell Rev. (April/May) (2006) 21.
[2] A. Bieberle-Hütter, D. Beckel, U.P. Mücke, J.L.M. Rupp, A. Infortuna, L.J. Gauckler, mstnews 12 (2005) 12.
[3] H. Huang, M. Nakamura, P. Su, R. Fasching, Y. Saito, F.B. Prinz, J. Electrochem. Soc. 154 (1) (2007) B20.
[4] C.D. Baertsch, K.F. Jensen, J.L. Hertz, H.L. Tuller, S.T. Vengallatore, S.M. Spearing, M.A. Schmidt, J. Mater. Res. 19 (9) (2004) 2604.
[5] Z.P. Shao, S.M. Haile, J. Ahn, P.D. Ronney, Z.L. Zhan, S.A. Barnett, Nature 435 (7043) (2005) 795.
[6] T.R. Dietrich, W. Ehrfeld, M. Lacher, M. Kramer, B. Speit, Microelectron. Eng. 30 (1–4) (1996) 497.
[7] D. Beckel, A. Dubach, A.R. Studart, L.J. Gauckler, J. Electroceramics 16 (3) (2006) 221.
[8] D. Beckel, U.P. Muecke, T. Gyger, G. Florey, A. Infortuna, L.J. Gauckler, Solid State Ionics 178 (5–6) (2007) 407.
[9] U.P. Muecke, PhD Thesis, ETH Zurich, Zurich, Switzerland (2007).
[10] U.P. Muecke, D. Beckel, A. Bieberle-Hütter, S. Graf, A. Infortuna, J.L.M. Rupp, J. Schneider, P. Mueller, A. Dommann, A. Bernard and L.J. Gauckler, Adv. Funct. Mater. (submitted for publication).
[11] D. Beckel, PhD Thesis, Thin Film Cathodes for Micro Solid Oxide Fuel Cell, ETH Zurich, Zurich, Switzerland (2007).
[12] V.T. Srikar, K.T. Turner, T.Y.A. Ie, S.M. Spearing, J. Power Sources 125 (1) (2004) 62.
[13] S. Rey-Mermet, P. Muralt, Materials and design study for micromachined solid oxide fuel cell membranes, in: E. Traversa (Ed.), Mater. Res. Soc. Symp. Proc., Materials Research Society (2007), pp. AA07–10.
[14] L. Madler, H.K. Kammler, R. Mueller, S.E. Pratsinis, J. Aerosol Sci. 33 (2) (2002) 369.
[15] W.J. Stark, L. Madler, M. Maciejewski, S.E. Pratsinis, A. Baiker, Chem. Commun. 5 (2003) 588.
[16] N. Hotz, M.J. Stutz, S. Loher, W.J. Stark, D. Poulikakos, Appl. Catal. B: Environ. 73 (3–4) (2007) 336.
[17] A.K. Chaniotis, D. Poulikakos, J. Power Sources 142 (1–2) (2005) 184.
[18] M.J. Stutz, N. Hotz, D. Poulikakos, Chem. Eng. Sci. 61 (12) (2006) 4027.
[19] M.J. Stutz, D. Poulikakos, Chem. Eng. Sci. 60 (24) (2005) 6983.
[20] A.F. Jankowski, J.P. Hayes, R.T. Graff, D. Morse, Micro-fabricated thin film fuel cells for portable power requirements, in: B.R. Schwarz, G. Ceder, S.A. Ringel (Eds.), Mat. Res. Soc. Symp. Proc. (2002), pp. V4.2.1–6.
[21] J.L.M. Rupp, A. Infortuna, L.J. Gauckler, Acta Mater. 54 (7) (2006) 1721.
[22] G. Robert, European Patent EP 1455409A1 (2004).
[23] S.B. Schaevitz, A. Franz, R. Barton, US 2006/0246333 A1 (2006).
[24] S.B. Schaevitz, A. Franz, R. Barton, A.P. Ludwiszewski, US 2006/0263655 A1 (2006).
[25] L.J. Gauckler, D. Beckel, U.P. Muecke, J.L.M. Rupp, WO2007/045113 (2007).
[26] L.J. Gauckler, D. Beckel, U.P. Muecke, J.L.M. Rupp, WO2007/045111 (2007).
[27] http://ccp.zhwin.ch/seses.